ACS OMEGA

Open Access

http://pubs.acs.org/journal/acsodf

Article

Screening of Methyl-β-cyclodextrins as an Antifading Agent for Cyanine Dye-Labeled Streptavidin to Improve the Performance of Genotyping Chips

Yuhao Ma,* Yun Fan, Xinyi Xu, Hongxia Li, Ruoyu Liu, and Chaojun Liu

Cite This: *ACS Omega* 2024, 9, 29491−29498

Read Online

ACCESS | Metrics & More | Article Recommendations | Supporting Information

ABSTRACT: As a photostabilizing agent for cyanine dye, methyl-β-cyclodextrin (MβCD) was investigated as a possible antifading agent for cyanine dye-labeled proteins. Cyanine-3 (Cy3)-labeled streptavidin (SA-Cy3) solutions containing MβCD exhibited improved resistance against photobleaching. Further research revealed that MβCD can be used as a coating material on the surface of gene chips. Chips loaded with cyanine dye (Cy3 and Cyanine-5 (Cy5))-conjugated model microbeads exhibited resistance against photobleaching with MβCD coatings. MβCD coatings improved the imaging quality of model chips and resulted in higher discrimination ratios (DR) of single base recognition by a set of control beads (NP68). In a whole genome genotyping assay for human samples, the MβCD-coated samples were found to have a better clustering performance than the noncoated ones for a group of randomly picked single nucleotide polymorphisms (SNPs).

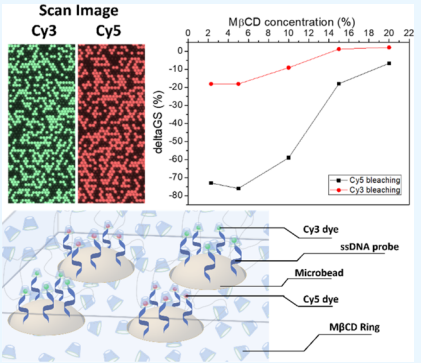

1. INTRODUCTION

Dyes or combinations of different dyes can be strong tools in various studies.[1−4] However, the use of fluorescence-based dyes was limited by photobleaching. Photo-oxidation of a cyanine dye occurs due to the formation of the triplet excited state, which is chemically active to ground-state oxygen to form oxygen radicals and then irreversibly causes fluorescence loss.[5] To avoid this unfavorable photophysical process that may hinder its wide applications, chemical agents such as 1,4-diazabicyclo[2.2.2]octane (DABCO),[6] *n*-propyl gallate (NPG),[7,8] and ascorbic acid have long been incorporated into the imaging medium as antifading agents. It has been suggested that antifading agents work by either removing reactive singlet oxygen generated by the quenching reaction of the triplet state fluorophore or by reduction to remove singlet oxygen.[9−11] Despite the abundance of antifading agents to choose from, the main drawback of many of them is the resulting lower fluorescence intensity.[7,12] For *in vitro* diagnostics based on imaging, the negatively affected fluorescence intensity could make weak signals more difficult to distinguish and therefore reduce assay sensitivity, which renders these potential fluorescence stabilizers less favorable options.

Researchers have found that the unique ring-like structure of cyclodextrin (CD) allows for the trapping of molecules with a hydrophobic moiety, which enables its applications in areas such as pharmaceutical, chemical, food, cosmetics, medical, and environmental industries.[13−19] For instance, CD has been used as a solubility enhancer in aqueous solutions[20] or to decrease toxicity[21−23] in the pharmaceutical industry. CD has been studied for encapsulation of cyanine dyes.[24,25] It has been proved that Cy3 dye can be efficiently encapsulated into β-CD and methyl-β-CD with interaction energies of −41.2 and −38.8 kcal/mol, respectively. Up to a 3-fold increase in the brightness of Cy3 was observed when Cy3 was complexed with methyl-β-CD, and a significant increase in photostability was determined for both complexes. It was suggested that the CD ring may shield the encapsulated dye from reactive species that may otherwise cause photobleaching.[24] Similarly, it was reported that a hydrophobic cyanine dye could form a conjugate with CD to achieve a higher photostability.[25]

Based on the aforementioned research, we further explored the potential of MβCD as a solution to the photobleaching of protein samples. Specifically, we focused on streptavidin, which was labeled with a cyanine dye and commonly used as a fluorescence probe to target specific areas of interest. As our research unfolded, we not only confirmed the effectiveness of MβCD in preventing photobleaching but also observed and discussed the differences in how MβCD interacts with the cyanine dye alone versus when it is conjugated with proteins. Additionally, we discovered that MβCD possesses good coating properties, resulting in a highly uniform and smooth

Received: March 3, 2024
Revised: June 2, 2024
Accepted: June 4, 2024
Published: June 27, 2024

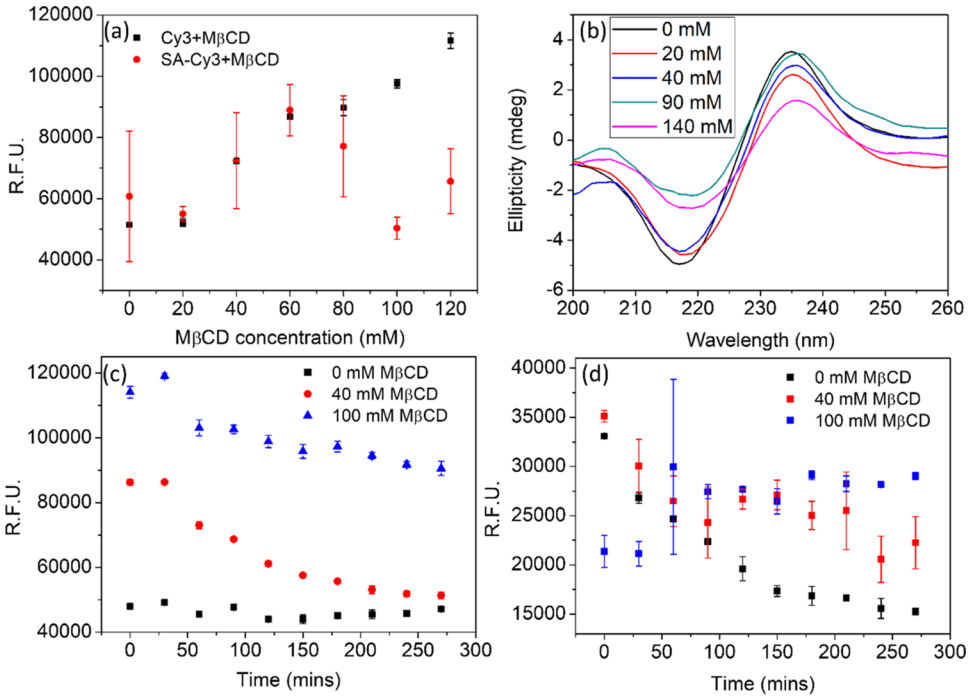

Figure 1. (a) Comparison of fluorescence intensity between unconjugated and SA-conjugated Cy3 dye complexed with MβCD at different MβCD concentrations. (b) Circular dichroism spectra of SA-Cy3 in the presence of MβCD at different concentrations. Fluorescence quenching profile of (c) unconjugated and (d) SA-conjugated Cy3 dye complexed with MβCD.

coating on the surface of the biochips. Genotyping chips coated with MβCD films were found with high antiphotobleaching properties and improved preservation of both Cyanine-3 (Cy3) and Cyanine-5 (Cy5) signals compared with those without MβCD. The imaging quality, discrimination ratios (DR) of model beads, and cluster separation scores (CSS) in human genome genotyping were assessed, and improved performance with MβCD films was proved.

2. EXPERIMENTAL SECTION

2.1. Materials. The cyanine dye (Cy3 and Cy5) and the streptavidin-conjugated form (SA-Cy3 and SA-Cy5) were provided by Shanghai BioScience Co., Ltd. Methyl-β-cyclodextrin (MβCD) was purchased from Adamas Reagent, Ltd. Polyacrylamide ($M_w \sim 10{,}000$) was purchased from Sigma-Aldrich Co., Ltd. All genotyping chips, custom-made oligonucleotides, and microbeads were provided by LASO Biotech Co., Ltd. (Soochow, China). Other chemicals and reagents were used as received without further treatment.

2.2. Measurements of Cyanine Dye Fluorescence in Solutions. To perform fluorescence measurements in aqueous medium, 150 μL of solution containing cyanine dye was mixed with 150 μL of MβCD solution in a 96-well microplate (Costar 96-well, nontreated, solid black plate); the concentration reported in the result has been corrected for dilution. The fluorescence was measured through a FLUOstar Omega microplate reader (BMG Labtech Co., Ltd.). To avoid oversaturation and ensure constant optical settings, the gain was set to 1048 for Cy3 reading and 2500 for SA-Cy3 reading. The excitation wavelength was set to 544 nm, and the emission range was set to 590 ± 10 nm. For the photobleaching test, an light-emittting diode (LED) illumination light source was used, and the exposure light power was controlled to 2 mW at 555 nm, as calibrated by an optical power meter.

2.3. Circular Dichroism Spectroscopy. The circular dichroism spectra were collected with a Chirascan-plus circular dichroism spectrometer (Applied Photophysics Ltd.). Prior to each measurement, the background spectrum was collected and subtracted from the sample curve. Each measurement scan was repeated 5 times at 25 °C with an accuracy of ±0.1 °C. Spectra were collected at a scan rate of 100 nm/min.

2.4. Preparation of MβCD Coatings on Genotyping Chips. The MβCD coating solution was prepared by dissolving MβCD in water at concentrations ranging from 2 to 20% along with the presence of 5 mM Tris (pH 8.0), 1.5% PAAm, and 0.02% methylchloroisothiazolinone. Dissolution of MβCD was done through vigorous shaking at 2500 rpm on an oscillator, followed by degassing through sonication for 15 min and centrifugation at 3000*g* for 5 min. Genotyping chips were incubated in the coating solution for 10 min at room temperature and then placed in a vacuum chamber for 2 h to dehydrate.

2.5. Photobleaching and Genotyping Tests. For the photobleaching test of genotyping chips, each chip was exposed to an external individual LED light source at a constant power of 4 mW for 2 h.

All chips were scanned separately on an OmniScan scanner (LASO Biotech Co., Ltd.) in the Cy3 and Cy5 channels. The grayscale value (GS) analysis and distinguishing rate determination for NP68 bead analysis were accomplished through OCS software v1.2.3 (LASO Biotech Co., Ltd.). The Cartesian plots for cluster analysis were made according to a previously reported method,[26] where R is the og-based normalized intensity and $\theta = (2/\pi) \times \arctan(B/A)$. The grouping algorithm to categorize plots into certain genotypes and the cluster separation score (CSS) value calculation were performed through MicroarrayDataWorkshop software v1.5 (LASO Biotech Co., Ltd.).

https://doi.org/10.1021/acsomega.4c02099
ACS Omega 2024, 9, 29491−29498

3. RESULTS AND DISCUSSION

3.1. Interaction of Cy3 Dye with MβCD. The influence of MβCD on the initial fluorescence and the effectiveness of MβCD in retarding photobleaching for both unconjugated and streptavidin-conjugated Cy3 dye were studied. For unconjugated Cy3 dye complexed with MβCD, the fluorescence intensity of Cy3 increases with the increased concentration of MβCD, when above a threshold MβCD concentration of 20 mM (Figure 1a). Approximately a 2-fold increase in intensity was achieved with an MβCD of 120 mM. A similar effect was also observed for the Cy5 dye/MβCD complex. Moreover, in contrast to what has been reported in the literature, we have found that a high MβCD concentration is critical in achieving the significantly increased intensity of Cy3, regardless of the concentration of Cy3 or the molar ratio of the host to dye. For a low MβCD concentration at the 2 mM level, we have observed no intensity change of Cy3, even with the same host-to-dye ratio of 1000:1 as the case in Figure 1a. For a high MβCD concentration at the 90 mM level, a host-to-dye ratio of 100:1 can still give a similar intensity increase (Figure S1). This result may suggest that an abundance of MβCD at a high concentration is necessary to maintain cyanine dye to reside in the MβCD host for most of the time, and the process of Cy3MβCD complexation is highly reversible with low binding affinity. Contrary to the case with unconjugated Cy3, Cy3 conjugated with SA has not shown an increase in initial fluorescence. The fluorescence intensity for SA-Cy3 remains almost unchanged throughout the whole concentration range of MβCD (Figure 1a). Such ineffective dye−host complexation is possibly due to steric hindrance by conjugated protein molecules.

Photostability testing was performed through fluorescence readings at different durations upon exposure to an external light source. Figure 1c gives the photostability plots of the Cy3/MβCD complex. It was surprising that almost no decrease in fluorescence throughout the process with Cy3 alone was present, suggesting a low quenching efficiency with the light exposure. However, complexation of Cy3 with MβCD, although showing an initial higher fluorescence, caused the fluorescence to decrease over time. In the case with 40 mM MβCD, a strong decrease of fluorescence quenching was observed and the fluorescence readings ultimately decreased to the extent slightly higher than that with no MβCD present. The quenching with 100 mM MβCD, in comparison, was much less in extent. Such a result seems to suggest that some extra photobleaching pressure was induced by the presence of MβCD, and a high MβCD concentration is able to balance this pressure. One possibility is that the highly reversible Cy3/MβCD complexation process induces some instability at the triplet excited states or increases the level of dye−oxygen interactions. As for the photostability plots of SA-Cy3 shown in Figure 1d, different trends were observed. Unlike unconjugated Cy3, SA-Cy3 without complexation with MβCD showed a gradual efficient fluorescence quenching during the period of light exposure, which indicates a different photostability profile compared with that of the pure dye. For SA-Cy3 complexed with 40 mM MβCD, the fluorescence is much less quenched, and with 100 mM MβCD, the fluorescence remains almost unchanged after 60 min of exposure. In comparison with the unconjugated dye, in which case MβCD may not be able to efficiently trap Cy3, it may interact with SA-Cy3 in a different way. The SA molecules may form a complex with MβCD and, therefore, indirectly form protections to Cy3 and then retard photobleaching.

To further explore the interaction between MβCD and SA-Cy3, the CD spectra of SA-Cy3 in the presence of MβCD were recorded (Figure 1b). The CD spectrum for streptavidin protein exhibited one peak at 232 nm and one valley at 216 nm, which indicates the predominant presence of β barrels.[27] For 20 and 40 mM MβCD, only some small spectrum variations appeared, under which circumstances the secondary structure of SA was mainly conserved. For samples with 90 mM, the ellipticity at 216 nm significantly decreased, while no severe change occurred for peaks at 232 nm. At a higher MβCD concentration of 140 mM, ellipticity decreased at both 216 and 232 nm. The result clearly suggests that significant protein denaturation occurred only with an MβCD concentration higher than a certain threshold value. In addition to the ellipticity changes of two characteristic SA peaks, we also noted that an extra peak appeared at around 205 nm, which might be ascribed to a certain structure pattern due to SA interacting with MβCD and is hard to determine without further studies. The strong changes in CD spectra of SA-Cy3 showed that MβCD may interact with SA protein and cause protein denaturation, with its hydrophobic cavity serving as a host to the protein hydrophobic moiety and unfolding its secondary structure.

3.2. Enhanced Imaging Performance with MβCD Coatings. With the inhibition of photobleaching of SA-Cy3 by MβCD being proved, it would be of interest to evaluate this performance with the fluorophores on the sample surface, as in the form of antifading mounting medium used in microscopy. The antifading properties of MβCD were tested through the formation of a coating layer on top of genotyping chips. The model DNA microarray was prepared by mixing and loading two types of microbeads on a microarray substrate, and each type of microbead had biotinylated oligonucleotide conjugated with either SA-Cy3 or SA-Cy5. Solutions of MβCD with different concentrations were cast on the chip surface and then dried as a thin layer of film under a vacuum. The initial and after-exposure images in both Cy3 and Cy5 channels were recorded, and ΔGS was used as a measure of photobleaching, which was obtained through the following equation

$$\Delta GS = \frac{GS_b - GS_a}{GS_a} \times 100\% \quad (1)$$

GS_a represents the average bead grayscale value of each fluorescence channel on one image before exposure, while GS_b represents the average bead grayscale value after exposure. The ΔGS results shown in Figure S2 revealed that Cy3 and Cy5 beads were photobleached to different extents. Although both Cy3 and Cy5 beads showed the same trend of decreased ΔGS with increased MβCD concentrations, at low MβCD concentrations from 2 to 10%, Cy5 beads were photobleached at a much larger scale than Cy3 beads. Under constant light exposure, the photobleaching rate of Cy5 was reported to be higher than that of Cy3,[28] which has been recognized as an issue in the comparability of lab-to-lab microarray experiment results.[29] The ΔGS for both Cy3 and Cy5 beads was decreased to a much lower level with an MβCD concentration over 15%, and for Cy3 beads, the obtained ΔGS was close to 0. The antifading property of MβCD on surface fluorophores was thus validated, similar to what we have obtained in solutions. Aside from the barrier effect against ground-state oxygen due to the

https://doi.org/10.1021/acsomega.4c02099
ACS Omega 2024, 9, 29491−29498

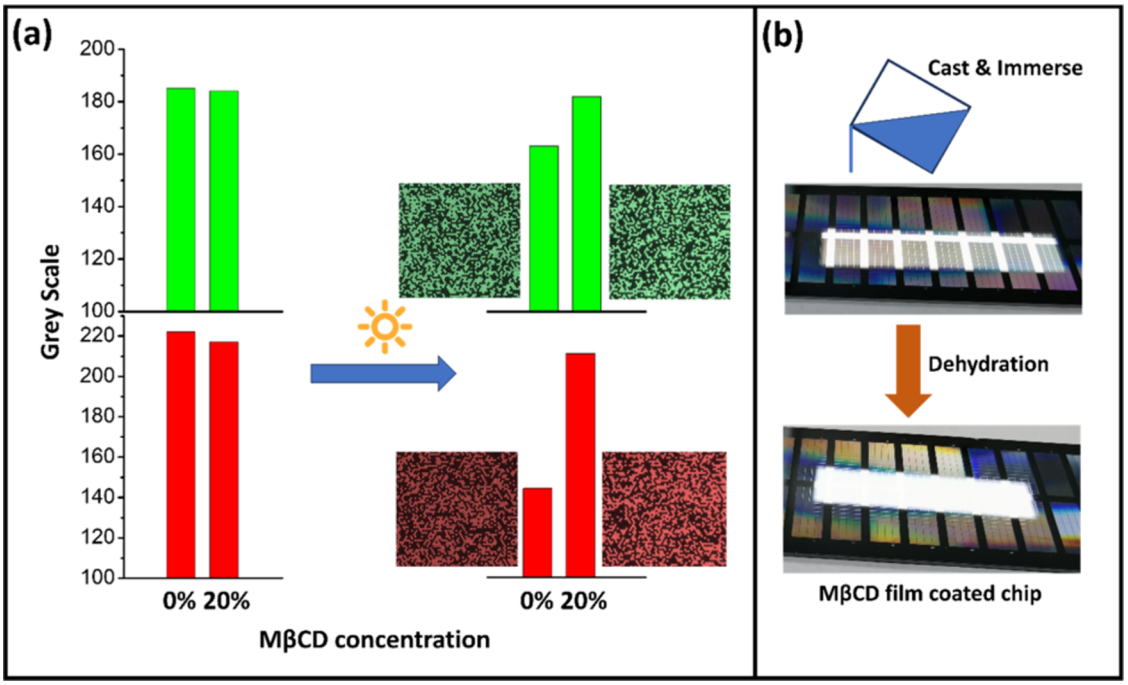

Figure 2. (a) Resistance of photobleaching of genotyping chips coated with a film containing 20% MβCD compared to 0% MβCD. (b) Process of MβCD-containing film formation on the genotyping chip surface.

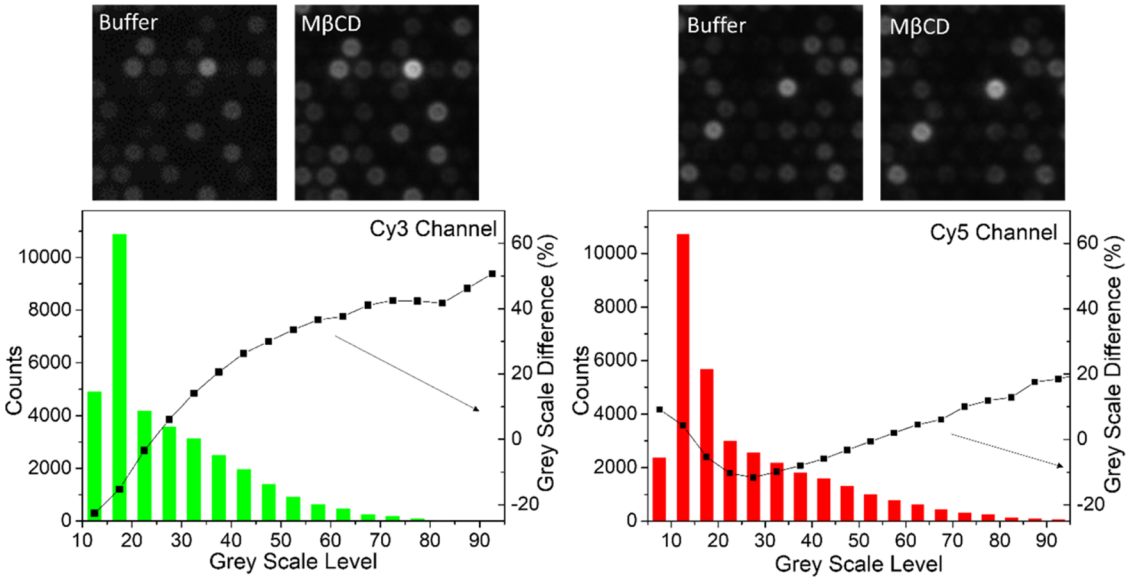

Figure 3. Representative scanned images (top) and statistic distribution (column) of grayscale values (bottom) of NP68 beads with imaging buffer and the averaged difference (square) in grayscale values for each level group between buffer and MβCD coating imaging in (bottom left) Cy3 channel and (bottom right) Cy5 channel.

formation of the MβCD/Cy3 or MβCD/Cy5 complex, it is also possible that the solidified film of immobilized MβCD isolates the fluorophores from atmosphere ozone, as an environmental photobleaching factor,[30] as we have noticed that the fluorescence images of coated genotyping chips maintained the same level of grayscale for both Cy3 and Cy5 even after several weeks, while the chips stored in the aqueous environment would experience rapid photobleaching, especially for Cy5, within 5 days. Aside from the photostabilizing properties, we also noticed that MβCD does have a significant influence on the film morphology. For an MβCD concentration lower than 5%, the formed film was uneven with the inner chip area thicker than the surrounding area. The films made with 5−20% MβCD give a shiny and smooth appearance with good toughness (Figure 2b). However, the films formed with over 20% MβCD become brittle and fragile and break easily to form cracks or cause pieces to flake off. It is obvious that a higher concentration of MβCD increases the solution viscosity, which would result in a thicker coating and changed coating properties; however, MβCD alone was not able to form a smooth and uniform coating. Therefore, a hydrophilic polymer was added to promote the film's smoothness. We believe that the long polymer chains provide sufficient hydrogen bonding sites for MβCD, whose molecules do not

https://doi.org/10.1021/acsomega.4c02099
ACS Omega 2024, 9, 29491−29498

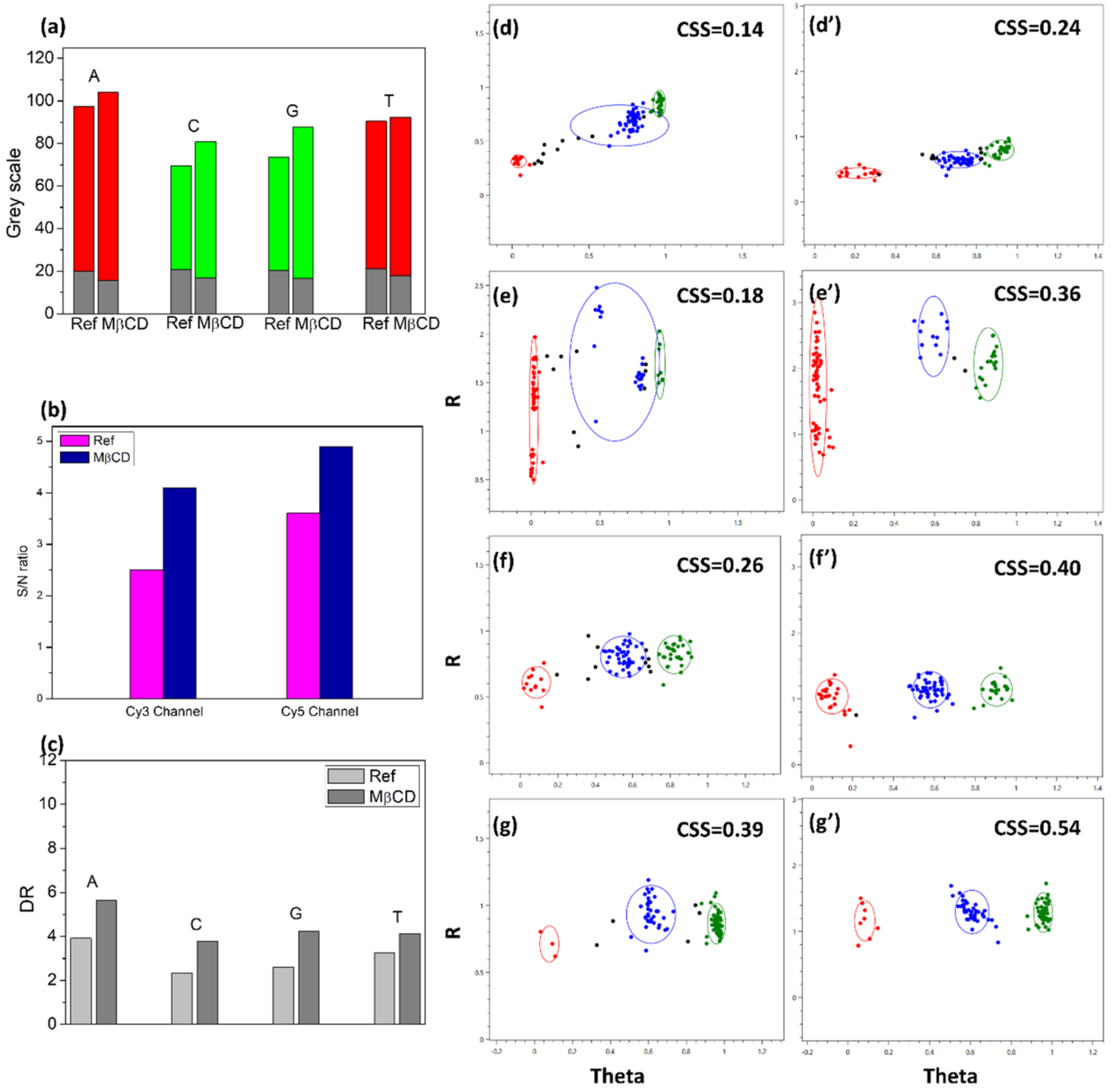

Figure 4. (a) Averaged signal and background grayscale values of each type of NP68 beads. (b) Signal-to-noise ratio of images to be analyzed in each fluorescence channel. The S/N in the Cy3 channel was defined as the ratio of CG bead GS to AT bead GS, and the S/N in the Cy5 channel was defined as the ratio of AT bead GS to CG bead GS. (c) DR values derived from grayscale data for NP68 beads. (d−g′) Representative Cartesian plots for cluster analysis and CSS values for selected *Homo sapiens* single nucleotide polymorphisms (SNPs): rs1621688 (d), rs379249 (e), rs10852734 (f), and rs11085118 (g) scanned with the imaging buffer, and the corresponding plots scanned with MβCD coatings (d′−g′). R is a log-based normalized grayscale value from both channels and $\theta = (2/\pi) \times \arctan(GS_{cy3}/GS_{cy5})$.

form intermolecular hydrogen bonding, and hereby serve as the media to evenly disperse MβCD upon dehydration, as shown in the graphic abstract.

In addition to the antifading properties, as expected, we also observed that the MβCD coating provides better image quality. Compared with the image taken under liquid buffer, as shown in Figure 3, the image taken with the MβCD coating exhibited a higher resolution with a sharper bead profile and brightness contrast. We believe that the MβCD coating has a higher refractive index (RI) over water and hence is more consistent with the RI of microbeads and substrate-forming material SiO_2 and is then better at channeling light into the camera sensor with less image blur caused by refraction.

The effect of the MβCD film on the performance of the controlled genotyping assay was evaluated. The genotyping beads for this control assay were prepared by immobilizing oligonucleotides with each probe sequence targeting a single nonpolymorphic nucleotide in the human genome. A total of 68 probe sequences (NP68) were thus designed (Table S1), covering all 4 possible bases. These 68 types of beads were

https://doi.org/10.1021/acsomega.4c02099
ACS Omega 2024, 9, 29491−29498

mixed homogeneously and loaded on LASO Biotech chips to form DNA microarrays, and the recognition of bead types was accomplished by a series of decoding processes prior to the genotyping assay.[31] The genotyping assay was performed through standard protocols provided by LASO Biotech, which mainly comprise the process of whole genome amplification (WGA), fragmentation, DNA denaturing, hybridization, single base extension, and staining. Microarray imaging was done either with a standard imaging buffer (Reference) or after coating of a MβCD film. For each recognized bead with the bead type validated, the discrimination ratio (DR) was defined by the ratio of the signal grayscale value, Cy5 for A and T and Cy3 for C and G, to the background grayscale value in the other channel.

Figure 4a shows the averaged signal and background grayscale values of all bead types targeting the same base, with the comparison between the reference and MβCD coating. It was revealed that the MβCD coating improved the assay signal-to-noise ratio by both increasing the signal grayscale values and decreasing the unwanted background intensity (Figure 4b) for all four bases. As a result, the DR values for all genotypes (A, C, G, and T) were improved. C and G genotypes were found with a higher DR increase over the A and T genotypes (Figure 4c). In addition to the photostabilizing properties of MβCD that contribute to the signal increase, it is very likely that the higher resolution works better at preserving the signal fluorescence while reducing the nonsignal grayscale value increase due to unfocused imaging. To verify this, the effect of MβCD on the grayscale values of beads was statistically analyzed. All recognized beads were subdivided into groups of different grayscale levels (bin width = 5), and the differences in grayscale values for each bead group between buffer and MβCD coating imaging were averaged (Figure 3), in which a positive value in percentage indicates higher grayscale values for MβCD-coated beads, and a negative value in percentage indicates higher grayscale values for beads under the imaging buffer. In the Cy3 channel, all group levels with a GS lower than 25 have decreased brightness with MβCD coatings. For group levels with a GS higher than 25, the brightness was increased with MβCD coatings, and the difference was larger with higher GS group levels. This observation coincided with the DR value change, as most of the beads with C, G genotypes have a signal Cy3 grayscale value over 25 and non-C, G genotypes have a background Cy3 grayscale value less than 25 (Table S2). In the Cy5 channel, however, the trend seems to be smaller and inconsistent. Only group levels with a GS from 15 to 55 showed a negative GS change with MβCD coatings, and group levels below or above this range showed a positive GS change. This also coincided with the DR values for A, T genotype beads, where most of the beads have the signal GS over 50 and most of the non-A, T genotype beads have the background GS falling in the range from 15 to 40 (Table S2). The relatively smaller GS change may suggest that the GS of beads in the Cy5 channel is less sensitive to the change in imaging media than that in the Cy3 channel, which should account for the small DR increase for A and T genotypes.

It is expected that the DR increase brought by MβCD coatings would improve the accuracy of algorithms, to better distinguish signal grayscale from background grayscale, and contribute to the genotyping accuracy for samples with unknown alleles. To verify this, we applied the MβCD coating to HSSA, a human whole genome genotyping chip provided by LASO Biotech Co., Ltd., which is capable of recognizing more than 83,000 SNPs. As most of the genotyping calls (>98.5%) are with CSS values higher than 0.3 and already have good genotyping cluster separations, we focused solely on the poorly separated calls with CSS values lower than or close to 0.3. A total of 50 such SNPs were randomly picked, and the cluster performance with and without MβCD coating was compared (Table S3). From Table S3, we noticed that most SNPs have a higher CSS with the MβCD coating. For many SNPs with poor cluster separation with CSS less than 0.3, remarkable increases in CSS over 0.3 were observed, which generally indicates good clustering performance and can give clear statistic separations among different genotypes. For SNPs with initial CSS scores close to 0.3, the improvement brought by the MβCD coating is less prominent than for the ones with a low initial CSS. Plots of four representative SNPs without and with the MβCD coating are shown in Figure 4. As is shown in the figure, the clusters of different genotypes obtained with the MβCD coating are farther separated from each other, with less overlapping regions between the homozygote and heterozygote, and therefore are less likely to generate ambiguous results (black dots) within these regions. The initial poor cluster separations for some SNPs could arise from a large DR variation among heterozygotes, which leads to a broad heterozygote domain within a wide θ range and region overlap (Figure 4d,e). The MβCD coating contributes to the narrowing down of DR variations and therefore provides better cluster separations.

Compared with other traditional antifading agents, MβCD in this study provides extra benefits by forming solidified films and allowing samples to be stored in the long term, while other reagents are to be used with aqueous media. We have also attempted to replace MβCD with other antifading agents, such as 1,4-diazabicyclo[2.2.2]octane (DABCO) and *n*-propyl gallate (NPG), and found that these chemicals have a negative influence on the film formation by salting out during the dehydration process, which can cause severe imaging issues.

4. CONCLUSIONS

In this study, we screened MβCD as a photostabilizer for cyanine dye-labeled SA. We proved that the presence of MβCD extended the lifetime of fluorescence of SA-Cy3 in solution during constant light exposure. Beyond this scope, we also proved that MβCD can be applied as an antiphotobleaching coating material for gene chips, which greatly reduces the loss of brightness of microbeads after 2 h of light irradiation at 4 mW. MβCD-coated genotyping chips were found with improved imaging quality and signal-to-background ratio compared to chips with aqueous imaging medium. Genotyping results showed that the cluster performance of some poorly genotyping SNPs can benefit from the MβCD coating. To our knowledge, this is the first time that MβCD has been used as coatings for gene microarray chips based on fluorescence imaging. This finding may as well have practical implications for other cyanine dye-involved applications.

■ ASSOCIATED CONTENT

Supporting Information

The Supporting Information is available free of charge at https://pubs.acs.org/doi/10.1021/acsomega.4c02099.

Fluorescence intensity of Cy3 enhanced by MβCD (Figure S1); photobleaching result of genotyping chips (Figure S2); list of probe sequences targeting non-

https://doi.org/10.1021/acsomega.4c02099
ACS Omega 2024, 9, 29491−29498

polymorphic nucleotide (NP68) in the human genome (Table S1); averaged grayscale values for NP68 microarray beads of controlled genotyping assay (Table S2); and cluster separation score (CSS) for 50 randomly picked SNPs (Table S3) (PDF)

AUTHOR INFORMATION

Corresponding Author

Yuhao Ma − *LASO Biotech, Soochow 215000, P. R. China*; orcid.org/0000-0001-7517-5786; Email: yma10@ualberta.ca

Authors

Yun Fan − *LASO Biotech, Soochow 215000, P. R. China*
Xinyi Xu − *LASO Biotech, Soochow 215000, P. R. China*
Hongxia Li − *LASO Biotech, Soochow 215000, P. R. China*
Ruoyu Liu − *LASO Biotech, Soochow 215000, P. R. China*
Chaojun Liu − *LASO Biotech, Soochow 215000, P. R. China*

Complete contact information is available at: https://pubs.acs.org/10.1021/acsomega.4c02099

Notes

The authors declare no competing financial interest.

ACKNOWLEDGMENTS

We would like to thank our colleagues in LASO Biotech for their contributions in oligo conjugation with microbeads, microarray preparation, decoding, library preparation, and data processing. We would also like to thank the staff members of Suzhou Institute of Nano-Tech and Nano-Bionics (SINANO), Chinese Academy of Sciences, for their support in sample characterizations.

REFERENCES

(1) Wang, J.; Ansari, A. A.; Malik, A.; Syed, R.; Ola, M. S.; Kumar, A.; AlGhamdi, K. M.; Khan, S. Highly Water-Soluble Luminescent Silica-Coated Cerium Fluoride Nanoparticles Synthesis, Characterizations, and In Vitro Evaluation of Possible Cytotoxicity. *ACS Omega* **2020**, *5* (30), 19174−19180.

(2) Khan, S.; Ansari, A. A.; Malik, A.; Chaudhary, A. A.; Syed, J. B.; Khan, A. A. Preparation, characterizations and in vitro cytotoxic activity of nickel oxide nanoparticles on HT-29 and SW620 colon cancer cell lines. *J. Trace Elem. Med. Biol.* **2019**, *52*, 12−17.

(3) Ansari, A. A.; Khan, S.; Aldalbahi, A.; Parchur, A. K.; Kumar, B.; Kumar, A.; Raish, M.; Rai, S. In-vitro cytotoxicity evaluation of surface design luminescent lanthanide core/shell nanocrystals. *Arabian J. Chem.* **2020**, *13* (1), 1259−1270.

(4) Khan, S.; Ansari, A. A.; Rolfo, C.; Coelho, A.; Abdulla, M.; Al-Khayal, K.; Ahmad, R. Evaluation of in vitro cytotoxicity, biocompatibility, and changes in the expression of apoptosis regulatory proteins induced by cerium oxide nanocrystals. *Sci. Technol. Adv. Mater.* **2017**, *18* (1), 364−373.

(5) Kanofsky, J. R.; Sima, P. D. Structural and environmental requirements for quenching of singlet oxygen by cyanine dyes. *Photochem. Photobiol.* **2000**, *71* (4), 361−368.

(6) Ouannes, C.; Wilson, T. Quenching of singlet oxygen by tertiary aliphatic amines. Effect of DABCO (1,4-diazabicyclo[2.2.2]octane). *J. Am. Chem. Soc.* **1968**, *90* (23), 6527−6528.

(7) Longin, A.; Souchier, C.; Ffrench, M.; Bryon, P. A. Comparison of anti-fading agents used in fluorescence microscopy: image analysis and laser confocal microscopy study. *J. Histochem. Cytochem.* **1993**, *41* (12), 1833−1840.

(8) Krenik, K. D.; Kephart, G. M.; Offord, K. P.; Dunnette, S. L.; Gleich, G. J. Comparison of antifading agents used in immunofluorescence. *J. Immunol. Methods* **1989**, *117* (1), 91−97.

(9) Gaigalas, A. K.; Wang, L.; Cole, K. D.; Humphries, E. Photodegradation of Fluorescein in Solutions Containing n-Propyl Gallate. *J. Phys. Chem. A* **2004**, *108* (20), 4378−4384.

(10) Rasnik, I.; McKinney, S. A.; Ha, T. Nonblinking and long-lasting single-molecule fluorescence imaging. *Nat. Methods* **2006**, *3* (11), 891−893.

(11) Widengren, J.; Chmyrov, A.; Eggeling, C.; Löfdahl, P.-Å.; Seidel, C. A. M. Strategies to Improve Photostabilities in Ultra-sensitive Fluorescence Spectroscopy. *J. Phys. Chem. A* **2007**, *111* (3), 429−440.

(12) Panchuk-Voloshina, N.; Haugland, R. P.; Bishop-Stewart, J.; Bhalgat, M. K.; Millard, P. J.; Mao, F.; Leung, W.-Y.; Haugland, R. P. Alexa Dyes, a Series of New Fluorescent Dyes that Yield Exceptionally Bright, Photostable Conjugates. *J. Histochem. Cytochem.* **1999**, *47* (9), 1179−1188.

(13) Crini, G. Review: A History of Cyclodextrins. *Chem. Rev.* **2014**, *114* (21), 10940−10975.

(14) Hajdu, C.; Gruiz, K.; Fenyvesi, É.; Nagy, Z. M. Application of cyclodextrins in environmental bioassays for soil. *J. Inclusion Phenom. Macrocyclic Chem.* **2011**, *70*, 307−313.

(15) Radu, C.-D.; Parteni, O.; Ochiuz, L. Applications of cyclodextrins in medical textiles—review. *J. Controlled Release* **2016**, *224*, 146−157.

(16) Buschmann, H.-J.; Schollmeyer, E. Applications of cyclodextrins in cosmetic products: A review. *J. Cosmet. Sci.* **2002**, *53* (3), 185−192.

(17) Devi, N. K. D.; Rani, A. P.; Javed, M.; Kumar, K.; Kaushik, J.; Sowjanya, V. Cyclodextrins in pharmacy-an overview. *Pharmacophore* **2010**, *1* (3), 155−165.

(18) Liu, Y.; Chen, Y.; Gao, X.; Fu, J.; Hu, L. Application of cyclodextrin in food industry. *Crit. Rev. Food Sci. Nutr.* **2022**, *62* (10), 2627−2640.

(19) Yu, G.; Jie, K.; Huang, F. Supramolecular Amphiphiles Based on Host−Guest Molecular Recognition Motifs. *Chem. Rev.* **2015**, *115* (15), 7240−7303.

(20) Saokham, P.; Muankaew, C.; Jansook, P.; Loftsson, T. Solubility of Cyclodextrins and Drug/Cyclodextrin Complexes. *Molecules* **2018**, *23* (5), No. 1161.

(21) Uzunova, V. D.; Cullinane, C.; Brix, K.; Nau, W. M.; Day, A. I. Toxicity of cucurbit[7]uril and cucurbit[8]uril: an exploratory in vitro and in vivo study. *Org. Biomol. Chem.* **2010**, *8* (9), 2037−2042.

(22) Rajewski, R. A.; Stella, V. J. Pharmaceutical applications of cyclodextrins. 2. In vivo drug delivery. *J. Pharm. Sci.* **1996**, *85* (11), 1142−1169.

(23) Irie, T.; Uekama, K. Pharmaceutical applications of cyclodextrins. III. Toxicological issues and safety evaluation. *J. Pharm. Sci.* **1997**, *86* (2), 147−162.

(24) Muddana, H. S.; Sengupta, S.; Sen, A.; Butler, P. J. Enhanced brightness and photostability of cyanine dyes by supramolecular containment. arXiv:1410.0844. arXiv.org e-Print archive. https://arxiv.org/abs/1410.0844 (submitted Oct 2, 2014).

(25) Guether, R.; Reddington, M. V. Photostable cyanine dye β-cyclodextrin conjugates. *Tetrahedron Lett.* **1997**, *38* (35), 6167−6170.

(26) Steemers, F. J.; Chang, W.; Lee, G.; Barker, D. L.; Shen, R.; Gunderson, K. L. Whole-genome genotyping with the single-base extension assay. *Nat. Methods* **2006**, *3* (1), 31−33.

(27) Kuo, T. C.; Lee, P. C.; Tsai, C. W.; Chen, W. Y. Salt bridge exchange binding mechanism between streptavidin and its DNA aptamer−thermodynamics and spectroscopic evidences. *J. Mol. Recognit.* **2013**, *26* (3), 149−159.

(28) Berlier, J. E.; Rothe, A.; Buller, G.; Bradford, J.; Gray, D. R.; Filanoski, B. J.; Telford, W. G.; Yue, S.; Liu, J.; Cheung, C.-Y.; et al. Quantitative comparison of long-wavelength Alexa Fluor dyes to Cy dyes: fluorescence of the dyes and their bioconjugates. *J. Histochem. Cytochem.* **2003**, *51* (12), 1699−1712.

(29) Von der Haar, M.; Preuß, J.-A.; Von der Haar, K.; Lindner, P.; Scheper, T.; Stahl, F. The impact of photobleaching on microarray analysis. *Biology* **2015**, *4* (3), 556−572.

(30) Fare, T. L.; Coffey, E. M.; Dai, H.; He, Y. D.; Kessler, D. A.; Kilian, K. A.; Koch, J. E.; LeProust, E.; Marton, M. J.; Meyer, M. R.; et al. Effects of atmospheric ozone on microarray data quality. *Anal. Chem.* **2003**, *75* (17), 4672−4675.
(31) Gunderson, K. L.; Kruglyak, S.; Graige, M. S.; Garcia, F.; Kermani, B. G.; Zhao, C.; Che, D.; Dickinson, T.; Wickham, E.; Bierle, J.; Doucet, D.; Milewski, M.; Yang, R.; Siegmund, C.; Haas, J.; Zhou, L.; Oliphant, A.; Fan, J. B.; Barnard, S.; Chee, M. S. Decoding randomly ordered DNA arrays. *Genome Res.* **2004**, *14* (5), 870−877.

https://doi.org/10.1021/acsomega.4c02099
ACS Omega 2024, 9, 29491−29498